Current Optics and Photonics
Vol. 4, No. 4, August 2020, pp. 353-360

ISSN: 2508-7266(Print) / ISSN: 2508-7274(Online)
DOI: https://doi.org/10.3807/COPP.2020.4.4.353

Development of a Microspot Spectroscopic Ellipsometer Using Reflective Objectives, and the Ellipsometric Characterization of Monolayer MoS_2

Sang Jun Kim[1], Min Ho Lee[1], and Sang Youl Kim[1,2]*

[1]*Ellipso Technology Co., Ltd., Suwon 16498, Korea*
[2]*Ajou University, Department of Physics, Suwon 16499, Korea*

(Received February 4, 2020 : revised April 23, 2020 : accepted May 11, 2020)

Adopting an elaborately designed reflective objective consisting of four mirrors, we have developed a rotating-polarizer-type microspot spectroscopic ellipsometer (SE) with an ultra-small spot size. The diameter of the focused beam, whether evaluated using a direct-image method or a knife-edge method, is less than 8.4 μm. After proper correction for the polarizing effect of the mirrors in the reflective objective, we unambiguously determine the dispersion of the complex refractive index and the thickness of monolayer MoS_2 using the measured microspot-spectroellipsometric data. The measured ellipsometric spectra are sensitive enough to identify small variations in thickness of MoS_2 flakes, which ranged from 0.48 nm to 0.67 nm.

Keywords : Microspot spectroscopic ellipsometer, Reflective objective, Complex refractive index, Monolayer MoS_2
OCIS codes : (120.2130) Ellipsometry and polarimetry; (120.3930) Metrological instrumentation; (310.6860) Thin films, optical properties

I. INTRODUCTION

Recently two-dimensional (2D) materials like graphene and transition-metal dichalcogenides (TMDs) have attracted intense research interest, due to their unusual physical properties [1-7]. In particular, TMD crystals display distinctive semiconducting properties at monolayer thickness. Their optical properties are important in verifying the transition to a direct-band-gap semiconductor, as well as their strong excitonic properties. Molybdenum disulfide (MoS_2) is the most studied 2D TMD. Contrary to graphene, MoS_2 is a semiconductor with nonzero band gap, and hence monolayer MoS_2 could complement graphene in many applications requiring thin, transparent semiconductors, such as optoelectronics and energy harvesting. Numerous reports have focused on the optical properties of MoS_2. Applying an extrapolation technique and a Kramers-Kronig analysis to its reflectivity spectrum, Beal and Hughes obtained the optical data for single-crystal 2*H*-MoS_2 [1]. Li *et al*. used a similar method to obtain the optical dielectric functions for exfoliated monolayer TMDs, and discussed the similarities and differences between the dielectric functions of monolayer TMDs and of the bulk materials [2]. Measurement of the optical constants of exfoliated single-layer TMDs was also carried out, adopting concerted frequency-dependent transmittance and reflectance measurements, and the measured optical constants were compared to those of bulk TMDs [3]. For the investigation of the optical absorption of single- and few-layer MoS_2 with high spatial resolution, a hyperspectral imaging technique was applied, and the optical properties with diffraction-limited spatial resolution were probed [4]. The spatially resolved reflectance technique or *microreflectance spectroscopy*, is well utilized to show a thickness-dependent bandgap and strong light-matter interaction in MoS_2 [5]. Energy-gap modulation by the number of MoS_2 layers was observed in the photoinduced voltage shift of top-gate phototransistors [6]. Meanwhile, exact evaluation of film thickness is critical

*Corresponding author: sykim@ajou.ac.kr, ORCID 0000-0001-5126-8291
Color versions of one or more of the figures in this paper are available online.

for an accurate determination of the complex dielectric function from measured reflectance spectra, especially for ultrathin films like monolayer MoS_2. The thickness of monolayer MoS_2 was simply estimated or identified by the optical contrast [3, 5, 6]. The interlayer spacing of bulk material was used, after being verified by Raman or photoluminescence spectroscopy [2]. In all cases, a small error in thickness determination results in a relatively large deviation from the actual complex dielectric function. An interesting report was made on the complex refractive index of synthesized monolayer MoS_2 based on the analysis of reflection contrast, while the thickness of a triangular MoS_2 island was measured by atomic force microscopy (AFM) [7, 8]. Direct thickness measurement of monolayer MoS_2 has been accomplished most often by AFM, with the reported thickness ranging from 0.65 to 0.83 nm [8-13].

Ellipsometry is a well-known technique, adequate for reliable characterization of ultrathin films. Spectroscopic ellipsometry is best suited for simultaneous determination of the complex optical dielectric function and thickness of ultrathin films, with high accuracy [14, 15]. However, when a conventional spectroscopic ellipsometer (SE) is used, due to the relatively large spot size (approximately 1.0 mm in diameter) the collected optical response has been averaged over a large area; hence the obtained optical properties and film thickness are also averaged over the same large measurement area. Thus the reported thickness for chemically exfoliated TMDs has ranged from ~1.0 to 4 nm, and the thickness of TMDs grown by vapor-phase sulfurization has ranged from 1.99 to 19.88 nm [16, 17]. Even an SE equipped with specially designed focusing optics has a spot about 100 μm in diameter, and it is considered that the reported optical properties of high-quality CVD-grown MoS_2 may not represent those of monolayer MoS_2 [18]. Meanwhile, the SE with the smallest spot can be found in the semiconductor industry, where it is desperately preferred. The diameter of the smallest spot available commercially at present is about 25 μm [19, 20]. In this manuscript, we introduce a microspot SE with carefully designed reflective objectives. The spot size of the proposed SE is small enough to fit into a triangular island of single-crystal monolayer MoS_2. The complex-refractive-index dispersion and thickness of CVD-grown crystalline monolayer MoS_2 are reported. The thickness variation of nominally monolayer MoS_2 flakes is also addressed.

II. MICROSPOT SE

Using an ordinary optical microscope, one can get a spot size of less than a micron without difficulty. The minimum spot size is limited by the diffraction of light, and is defined in terms of the wavelength of light λ and the numerical aperture (NA) of an objective, as $\sim\lambda$/NA. Thus a number of optical-microscope objectives that give spots of less than a few tenths of a micron in diameter are available commercially. On the other hand, the diameter of the smallest spot available in commercial SE at present is about 25 μm [19, 20]. It can be elongated by a factor of about 3 on the sample surface, when the angle of incidence is 70°. This large spot size of SE comes from the following two restrictions: The first is that the spectral range in SE covers from vacuum ultraviolet (VUV) to near infrared (NIR), and the available materials that are transparent and can be used as a focusing lens over this wide range are quite limited. The second restriction is simple, but more profound. In SE, the light is incident obliquely, mostly making an angle of ~70° from the surface normal. Thus for the housing of an objective not to touch the sample surface, the objective should have a sufficiently long working distance. A focusing objective with a very long working distance and that covers the wide spectral range from VUV to NIR is a necessity for microspot SE at the target. In addition, a focusing objective with coaxial structure is not favored, since it would yield a highly focused beam on the sample surface, which would make it difficult to define the angle of incidence. To overcome these obstacles, a focusing objective composed of four reflecting mirrors is introduced in the present work. The developed objective does not have any transmitting element, so it is free from chromatic aberration. The position and curvature of each mirror are strictly custom-designed to fit the positions of light source, sample, and detector of an existing spectroscopic ellipsometer. The optical path length of both polarizer and analyzer are also taken into account. The magnification ratio and NA of the custom-designed objective are 10× and 0.1 respectively. The mirrors are made of aluminum and are coated with a thin film of MgF_2. Two focusing objectives are placed symmetrically around the sample: one between the rotating polarizer and the sample, and the other between the sample and the fixed analyzer [21]. In Fig. 1, a schematic diagram of the two focusing objectives is shown, with one of the four reflecting mirrors enlarged. A similar coaxially folded, all-reflective optical system has been reported [22], but it is designed for imaging, and its working wavelength is 450-750 nm.

The polarization state of light is changed upon reflection, unless the angle of incidence is zero. The developed microspot SE has two focusing objectives, or eight reflecting surfaces, and their effect on the polarization state of light is not trivial. Two key elements that influence the polarization state upon reflection are 1) the angle of incidence and 2) any coating on the aluminum reflecting surface. The most significant effect comes from the second mirror from the sample surface in each objective: The radius of curvature of this mirror is the smallest (about 5 mm), and the angle of incidence at its surface is the largest. The reflection coefficient of a *p*-wave at this surface is quite different from that of an *s*-wave, and hence the polarization state of the reflected light changes significantly. Other mirrors introduce similar changes of polarization state cumulatively,

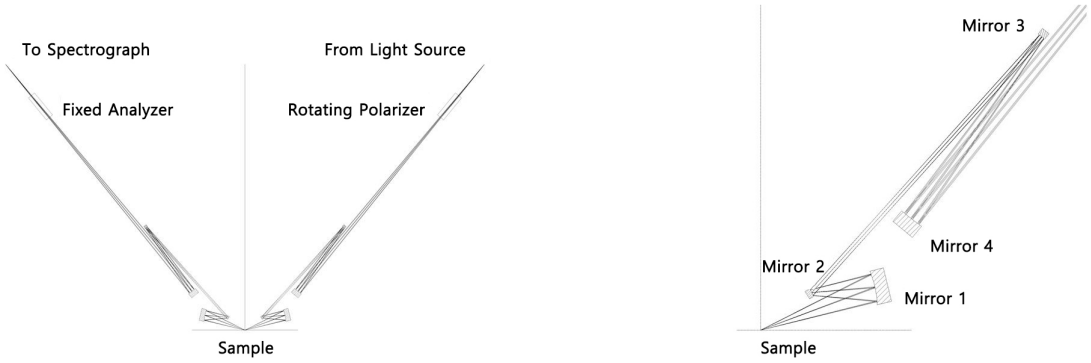

(a) (b)

FIG. 1. (a) A schematic diagram of two focusing objectives composed of four reflecting mirrors each, and (b) an enlarged schematic diagram of the four reflecting mirrors in the objective between the sample and the rotating polarizer.

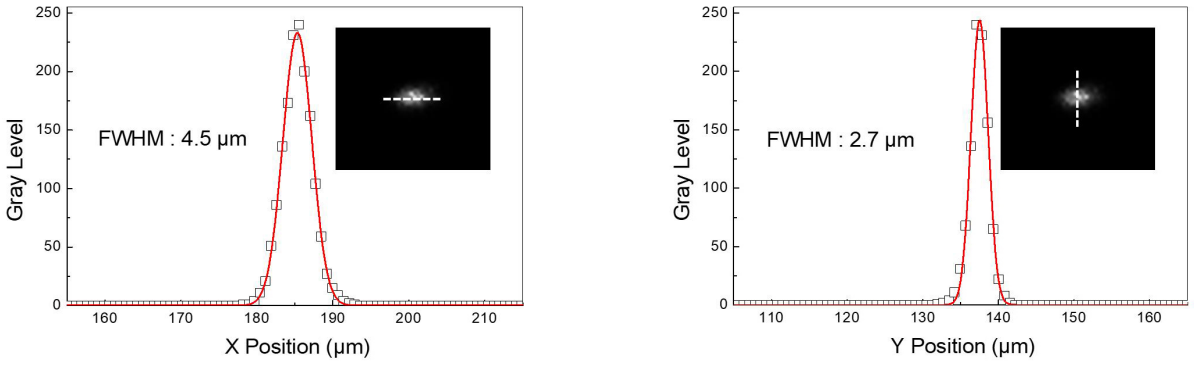

(a) (b)

FIG. 2. The image of the smallest spot looks like an elongated ellipse. The diameters of the spot are given as (a) 7.6 μm along the semimajor axis and (b) 4.7 μm along the semiminor axis.

but in lesser amounts. Thus the polarizing effect of eight reflecting mirrors distorts the polarization-state change originating from the reflection from the sample surface. Without a proper treatment of the polarizing effect of these reflecting surfaces, the analysis based on the measured ellipsometric data will be distorted accordingly. In the following sections, a method to take the polarizing effect of the objectives into account is addressed, after the explanation of spot-size measurement.

The light emitted from one end of an optical fiber is focused by the proposed reflective objective; the other end of the fiber is illuminated by a collimated beam from a 75-W Xe arc lamp. Since the diameter of the fiber is 50 μm and the magnification ratio of the present objective is 10×, the expected diameter of the spot at the sample position is 5 μm. The measured spot size was greater than the expected one, however. Both an image method and a knife-edge method are independently used to measure the spot size at the sample position.

2.1. Image Method

A CCD camera and zoom optics are installed to capture the image of the focused beam. The zoom function is useful for getting an image of the spot as the imaging plane is moved along the optical axis. At each pixel of the captured image, the grayscale level is converted to a value from 0 to 255. The gray level converted to a number shows a Gaussian-like distribution along a line crossing the center of the spot. The diameter of a spot is defined as the width corresponding to $1/e^2$ of the peak intensity, which is about 1.7 times the full width at half maximum (FWHM) of the best-fit Gaussian distribution function [23]. The spot size decreases to its smallest value at the focal plane, and increases as the imaging plane is moved away from the focal plane. The image at the smallest spot is not a circle, due to the off-axis configuration of the reflective objective; rather, it looks like an elongated ellipse, and thus two diameters are obtained, one along the semimajor axis and the other along the semiminor axis. The area of the elongated ellipse obtained from the smallest image is about 4.7×7.6 μm^2 as shown in Fig. 2.

2.2. Knife-edge Method

Independently, the spot size is measured using a knife-edge method. A light-blocking half-plane, like the straight edge of a knife or other blade, is progressively moved

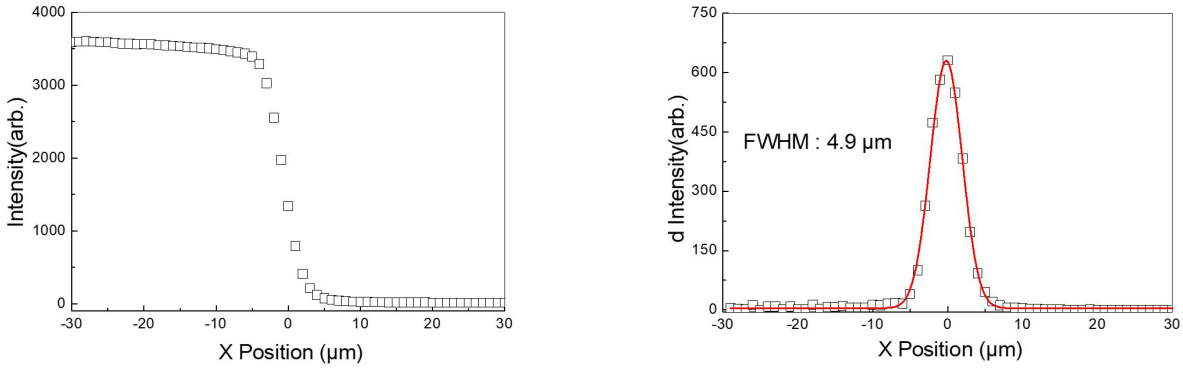

(a) (b)

FIG. 3. (a) The intensity of the transmitted light and (b) its derivative with respect to the travel distance of the knife edge at the position of the smallest spot (open squares). The best-fit Gaussian distribution function to the differentiated intensity is shown for comparison (solid line). The spot size is determined as 8.4 μm.

along the direction perpendicular to the beam path. The intensity of light is collected while the knife edge is being moved. After that, the position of the knife edge is shifted along the direction parallel to the beam path, and again the intensity of light is collected while the knife edge is being moved. This procedure is repeated for a distance long enough to cover the whole beam-waist region. The intensity of light collected at each knife-edge position along the perpendicular direction shows a Gaussian shape when it is differentiated with respect to the travel distance of the knife edge. The best-fit procedure to a Gaussian distribution function is also executed, and the spot size is obtained by multiplying the FWHM by 1.7. The smallest value among the sizes collected for all knife-edge positions is defined as the spot size of the focused beam. The spot size of the focused beam determined via this knife-edge method is 8.4 μm. The intensity of light and the differentiated intensity for the smallest spot are shown in Fig. 3, together with the best-fit Gaussian curve.

The straightness of the knife edge is critical when one applies this method to measure a spot as small as ~10 μm. A knife with a rough edge is an apparent source of error, such that a sawtooth-shaped edge with about 1.0 μm of roughness would result in a measured spot size larger than the actual one by about 1.0 μm. Using an optical microscope, we observed that the knife has about this magnitude of roughness to its edge, and hence we think that the measured spot size using this knife-edge method is larger than the actual one by ~1.0 μm.

2.3. Polarizing Effect of Reflective Objectives

As mentioned above, the effect of eight reflecting surfaces in two focusing objectives on the polarization state of light is not trivial. In this manuscript, we introduce the concept of a pseudosample, composed of the sample of interest and eight reflecting surfaces, for a proper treatment of the polarizing effect of these reflecting surfaces. We derive the expressions for the pseudoellipsometric constants ψ_μ and Δ_μ of this pseudosample, in terms of the ellipsometric constants of the sample and the parameters representing the polarizing effect of reflecting surfaces. After that, we apply the conventional modeling technique to these pseudo-ellipsometric constants; that is, we minimize the error function based on these pseudoellipsometric constants to determine the unknown parameters of the sample.

Let $\mathbf{M}_1$, $\mathbf{M}_2$, $\mathbf{M}_3$, and $\mathbf{M}_4$ be the Jones matrices representing the polarizing action of each reflecting surface in one objective. The polarizing effect of the objective on the polarizer side can be expressed as $\mathbf{M}_P = \mathbf{M}_1 \cdot \mathbf{M}_2 \cdot \mathbf{M}_3 \cdot \mathbf{M}_4$, and that on the analyzer side as $\mathbf{M}_A = \mathbf{M}_4 \cdot \mathbf{M}_3 \cdot \mathbf{M}_2 \cdot \mathbf{M}_1$. Let us denote the Jones matrix of a sample as $\mathbf{S}$; then the pseudo-Jones matrix $\mathbf{S}_\mu$ of the sample is defined as appears below.

$$\mathbf{S}_\mu = \mathbf{M}_A \cdot \mathbf{S} \cdot \mathbf{M}_P . \tag{1}$$

Since the reflecting surface is isotropic, there is no crosstalk between *p*-wave and *s*-wave components upon reflection. Hence one can write the Jones matrix of the j^{th} reflecting surface as $\mathbf{M}_j = \begin{pmatrix} \tan\psi_j e^{i\Delta_j} & 0 \\ 0 & 1 \end{pmatrix}$ ($j = 1, 2, 3, 4$). Then, utilizing the relation $\mathbf{M}_P = \mathbf{M}_A^T \equiv \mathbf{M}$ together with the relation $\mathbf{M} \cdot \mathbf{M}^T = \begin{pmatrix} \tan^2\psi_M e^{i\Delta_{2M}} & 0 \\ 0 & 1 \end{pmatrix}$, one obtains the following expressions for the pseudoellipsometric constants:

$$\tan\psi_\mu = \tan\psi \tan^2\psi_M , \tag{2}$$

$$\Delta_\mu = \Delta + \Delta_{2M} . \tag{3}$$

ψ_M and Δ_{2M} can be called the effective ellipsometric constants of the two objectives, and they can be determined by either calculation or measurement. When the angle of incidence and the film coated on every reflecting surface are known, one can calculate ψ_M and Δ_{2M}. On the other

hand, when a standard reference material (SRM) is given, one can determine ψ_M and Δ_{2M} by inverting Eqs. (2) and (3) using the measured ellipsometric spectra of the SRM. In this work, the latter method is adopted. The best SRM for this purpose is air in straight-through operation (STO). In the configuration of STO, the angle of incidence is 90° and $r_p = r_s$. Thus $\psi = 45^\circ$ and $\Delta = 0^\circ$, and the measured ellipsometric constants $\psi_{\mu STO}$ and $\Delta_{\mu STO}$ of air in STO are related to ψ_M and Δ_{2M} as follows:

$$\tan^2 \psi_M = \tan \psi_{\mu STO}, \tag{4}$$

$$\Delta_{2M} = \Delta_{\mu STO}. \tag{5}$$

Since the proposed microspot SE has the configuration of polarizer-sample-analyzer and operates as a rotating-polarizer-type SE, the conventional calibration procedure based on the residual-minimization method is adopted [15]. It is emphasized that since either *p*-wave or *s*-wave is the eigenstate of polarization of two focusing objectives, the conventional residual calibration procedure can be directly applied to this microspot SE without any modification. After the polarizer starting angle P_0 and the analyzer starting angle A_0 are determined, the ellipsometric constants $\psi_{\mu STO}$ and $\Delta_{\mu STO}$ of air are collected in the STO configuration. These ellipsometric constants are used to calculate the pseudo ellipsometric constants ψ_μ and Δ_μ in Eqs. (2) and (3) with the help of Eqs. (4) and (5).

The pseudoellipsometric spectra α_μ and β_μ are measured for three samples: a bare silicon wafer, crystalline silicon with 100-nm-thick oxide on it, and crystalline silicon with 200-nm-thick oxide on it. In Fig. 4 the spectra are compared to the best-fit simulated ones, 1) without the polarizing effect of reflecting surfaces and 2) with the polarizing effect of reflecting surfaces, respectively. One can easily verify that the fits to the measured ellipsometric spectra become excellent when the polarizing effect of reflecting surfaces is properly taken into account [24]. The oxide thickness can be determined following the best-fit modeling procedure [15]. For the 100-nm-thick oxide sample, it appears to be 100.46 ± 0.008 nm, which is quite close to the 99.35 ± 0.004 nm determined by using a conventional spectroscopic ellipsometer. The small difference of approximately 1.1 nm can be reduced to nearly zero after finer tuning of the proposed microspot SE. The pseudo ellipsometric spectra α_μ and β_μ are related to ψ_μ and Δ_μ as follows:

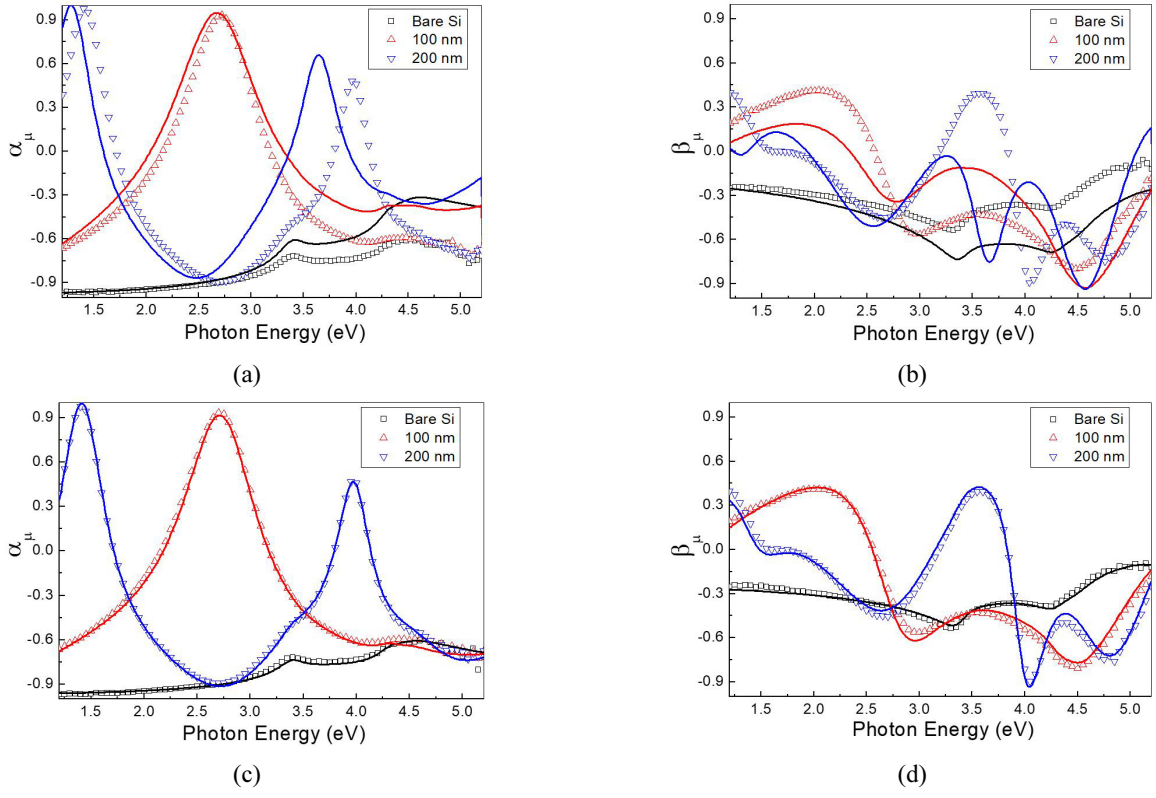

FIG. 4. (a) The measured ellipsometric spectra α_μ (open symbols) and best-fit simulation (solid lines) without considering the polarizing effect of reflecting surfaces in objectives, and (b) likewise β_μ, for bare silicon (black squares), crystalline silicon with 100-nm-thick oxide (red upright triangles), and crystalline silicon with 200-nm-thick oxide (blue inverted triangles), respectively. When the polarizing effect of reflecting surfaces is taken into account, the best fits to the measured ellipsometric spectra (c) α_μ and (d) β_μ become excellent.

$$\alpha_\mu = \frac{\tan^2\psi_\mu - 1}{\tan^2\psi_\mu + 1}, \tag{6}$$

$$\beta_\mu = \frac{2\tan\psi_\mu \cos\Delta_\mu}{\tan^2\psi_\mu + 1}. \tag{7}$$

III. ELLIPSOMETRIC CHARACTERIZATION OF MONOLAYER MoS_2

MoS_2 monolayers are grown via chemical vapor deposition (CVD) on a silicon substrate with a 296-nm-thick layer of SiO_2. MoS_2 monolayers with lateral sizes ranging from a few to about 25 μm grow, mostly in triangular shapes as shown in Fig. 5. Since the obliquely incident beam on a sample surface is elongated, the spot size to fit within monolayer MoS_2 of ~25 μm should be less than 10 μm. In this work, using the developed microspot SE, we place the entire probing spot inside of a triangular MoS_2 monolayer.

Based on the triangular shape of the MoS_2 flakes monitored by optical microscopy [13], a crystalline monolayer MoS_2 is carefully selected and the spectro-ellipsometric measurements are made at an incident angle of 70° in the spectral range of 1.2 to 4.5 eV. We characterize the monolayer MoS_2 in two steps. First, to get the thickness of SiO_2, we make an ellipsometric measurement and perform

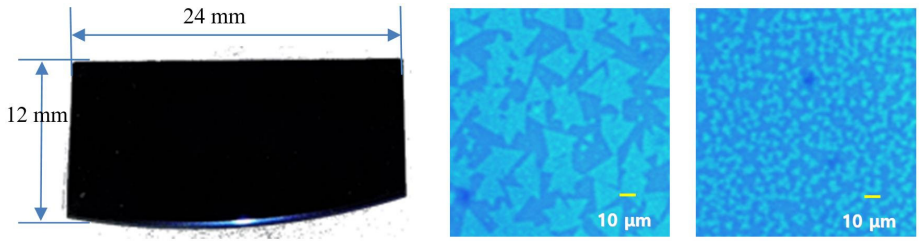

FIG. 5. (a) MoS_2 flakes grown on a SiO_2/c-Si substrate via the CVD method, and (b and c) enlarged views. The MoS_2 monolayers are mostly in triangular shapes with sizes ranging from a few to ~25 micrometers.

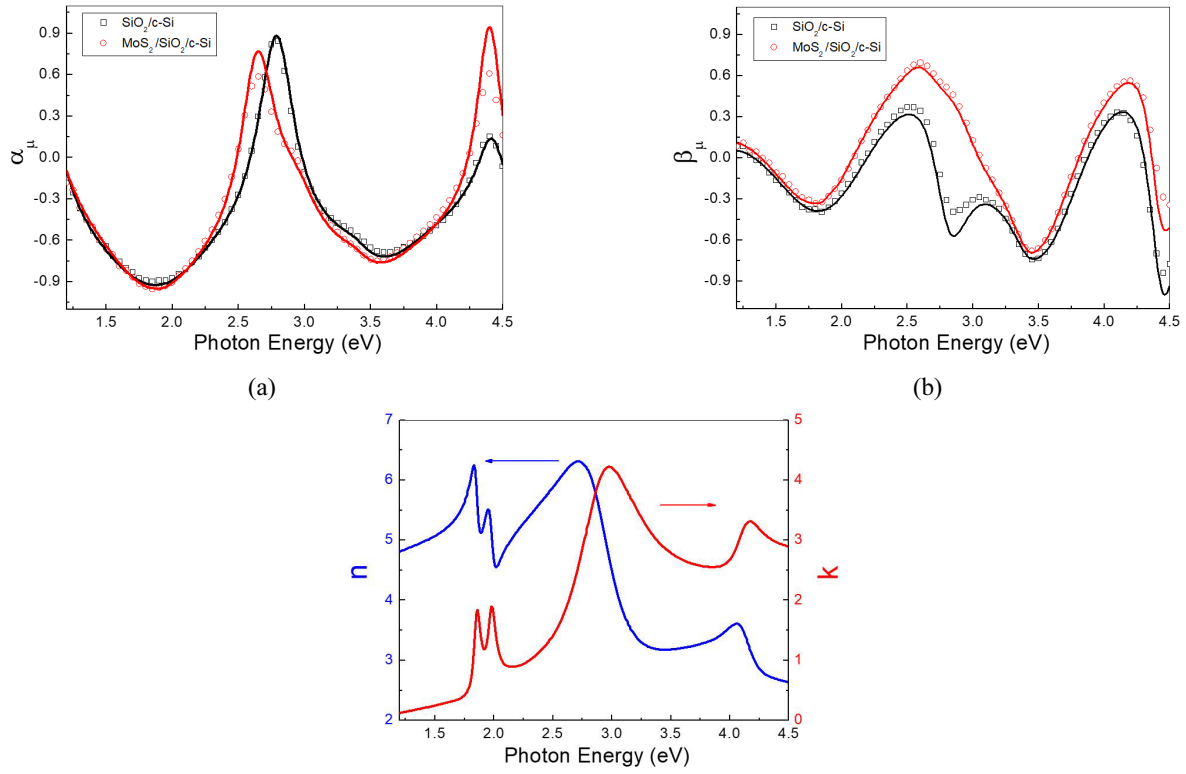

FIG. 6. (a and b) The measured spectra of the pseudoellipsometric constants α_μ and β_μ for the silicon substrate with oxide (black open squares) and those for the crystalline monolayer MoS_2 coated on it (red open circles). The best-fit simulations are shown as solid lines. (c) The dispersion of the complex refractive index of the crystalline monolayer MoS_2, as determined in this study.

the modeling analysis at a position a few tens of micrometers from the MoS_2 monolayer of interest. The thickness of the SiO_2 just beside the MoS_2 monolayer of interest is used as that of the SiO_2 beneath the MoS_2 monolayer of interest. Although a variation in SiO_2 thickness of less than 1.0 nm has a negligible effect on the analysis of the MoS_2 monolayer, this procedure is included to get the exact thickness of SiO_2 and to minimize any possible uncertainty that might come from an incorrect implication of SiO_2 thickness. After that, the spectroellipsometric data are collected for the MoS_2 monolayer of interest, and the thickness and complex-refractive-index dispersion of the monolayer MoS_2 are simultaneously determined. The Tauc-Lorentz dispersion equation with six oscillators is used to represent the complex-refractive-index dispersion of MoS_2. Two oscillators are solely dedicated to the two excitons sharply peaked at 1.86 and 1.98 eV. Typical spectra of the pseudoellipsometric constants α_μ and β_μ for the silicon substrate with oxide appear in Fig. 6. The spectra of the pseudoellipsometric constants for the crystalline monolayer MoS_2 on silicon substrate, together with the best-fit simulation are also plotted for close comparison. As can be seen clearly, a very thin layer of MoS_2 makes a huge difference to both α_μ and β_μ. This sensitivity of α_μ and β_μ implies that the thickness and the dispersion of the complex refractive index of a MoS_2 monolayer can be determined unambiguously. The determined thickness is 0.50 nm, and the dispersion of the complex refractive index is plotted in Fig. 6(c).

It is observed that the ellipsometric constant α_μ varies sensitively with MoS_2 thickness in the spectral region 1) around 2.6 eV, as a redshift of peak position accompanied by a decrease in peak height, and 2) around 4.0 eV, as a decrease of shoulder level. The ellipsometric constant β_μ also varies sensitively with MoS_2 thickness over a broader spectral region around both 2.6 eV and 4.2 eV. This sensitivity of α_μ and β_μ enables us to identify a very small thickness variation in monolayer-seeming MoS_2 flakes. Three typical MoS_2 flakes are selected to identify the thickness variation, in connection with their optical micrographs. The measured ellipsometric spectra and analysis results are shown in Fig. 7. The thickness of the MoS_2 flakes ranges from 0.48 to 0.67 nm, which is accompanied by the shape deviation of flakes from an equilateral triangle to a bent one, or to a starfish shape [13].

IV. SUMMARY AND CONCLUSIONS

Adopting carefully designed reflective objectives, we develop a rotating-polarizer-type microspot spectroscopic ellipsometer (μ-spot SE). The focusing objective is composed of four reflecting mirrors. The position and curvature of each mirror are strictly custom-designed to fit the configuration of light source, sample, and detector of an existing spectroscopic ellipsometer. The optical path lengths of polarizer and analyzer are also taken into account. The spot size is measured using both an image method and a knife-edge method. The evaluated diameter of the spot is approximately 8.4 μm, which is small enough to fit into a

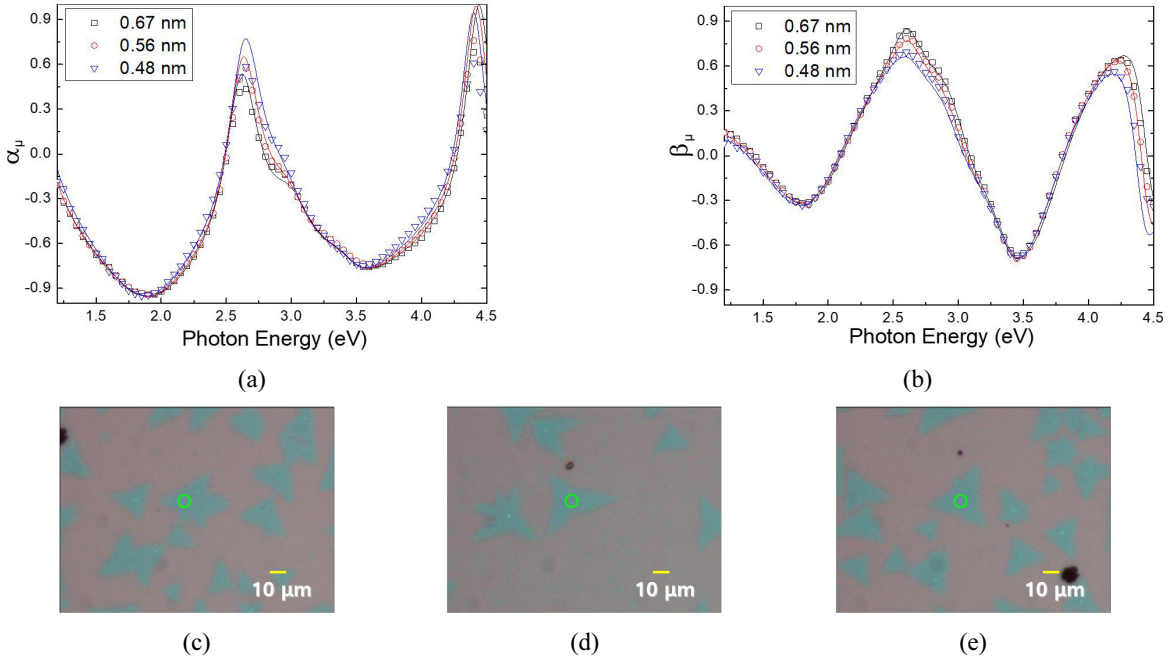

FIG. 7. The measured spectra of the pseudoellipsometric constants (a) α_μ and (b) β_μ of three typical MoS_2 flakes are shown as symbols and the corresponding best fits as solid lines. The determined thicknesses of the MoS_2 flakes are (c) 0.67 nm, (d) 0.56 nm, and (e) 0.48 nm. The green circles indicate the measured locations.

triangular island of crystalline monolayer MoS_2. After proper correction for the polarizing effect of the eight reflecting mirrors in two objectives, this μ-spot SE is utilized to determine the complex-refractive-index dispersion and the thickness of CVD-grown crystalline monolayer MoS_2. The Tauc-Lorentz dispersion equation with six oscillators is used to describe the complex-refractive-index dispersion of MoS_2. Utilizing the sensitivity of ellipsometric spectra to the thickness of monolayer MoS_2 around 2.6 eV and 4.0-4.2 eV, the thickness variation of an MoS_2 flake is addressed in connection to its shape. The thickness tends to increase from 0.48 nm to 0.67 nm as the shape of the flake deviates from an equilateral triangle to a bent one, or to a starfish shape. This μ-spot SE can be quite useful to researchers interested in optical characterization of micrometer-sized two-dimensional materials.

ACKNOWLEDGMENT

The authors would like to thank Prof. Ji-Yong Park of Ajou University for providing the CVD-grown MoS_2 samples, and Dr. Jin-Ho Jung of Prooptics for customizing the reflective objectives. This study was supported by the Korea Evaluation Institute of Industrial Technology (Project Number: 10067487).

REFERENCES

1. A. R. Beal and H. P. Hughes, "Kramer-Kronig analysis of the reflectivity spectra of 2H-MoS_2, 2H-$MoSe_2$ and 2H-$MoTe_2$," J. Phys. C: Solid State Phys. **12**, 881 (1979).
2. Y. Li, A. Chernikov, X. Zhang, A. Rigosi, H. M. Hill, A. M. van der Zande, D. A. Chenet, E.-M. Shih, J. Hone, and T. F. Heinz, "Measurement of the optical dielectric function of monolayer transition-metal dichalcogenides: MoS_2, $MoSe_2$, WS_2, and WSe_2," Phys. Rev. B **90**, 205422 (2014).
3. Y. V. Morozov and M. Kuno, "Optical constants and dynamic conductivities of single layer MoS_2, $MoSe_2$, and WSe_2," Appl. Phys. Lett. **107**, 083103 (2015).
4. A. Castellanos-Gomez, J. Quereda, H. P. van der Meulen, N. Agraït, and G. Rubio-Bollinger, "Spatially resolved optical absorption spectroscopy of single- and few-layer MoS_2 by hyperspectral imaging," Nanotechnology **27**, 115705 (2016).
5. C. Hsu, R. Frisenda, R. Schmidt, A. Arora, S. M. de Vasconcellos, R. Bratschitsch, H. S. J. van der Zant, and A. Castellanos-Gomez, "Thickness-dependent refractive index of 1L, 2L, and 3L MoS_2, $MoSe_2$, WS_2, and WSe_2," Adv. Opt. Mater. **7**, 1900239 (2019).
6. H. S. Lee, S.-W. Min, Y.-G. Chang, M. K. Park, T. Nam, H. Kim, J. H. Kim, S. Ryu, and S. Im, "MoS_2 nanosheet phototransistors with thickness-modulated optical energy gap," Nano. Lett. **12**, 3695-3700 (2012).
7. H. Zhang, Y. Ma, Y. Wan, X. Rong, Z. Xie, W. Wang, and L. Dai, "Measuring the refractive index of highly crystalline monolayer MoS_2 with high confidence," Sci. Rep. **5**, 8440 (2015).
8. T. Han, H. Liu, S. Wang, S. Chen, W. Li, X. Yang, M. Cai, and K. Yang, "Probing the optical properties of MoS_2 on SiO_2/Si and sapphire substrates," Nanomaterials **9**, 740 (2019).
9. M. M. Benameur, B. Radisavljevic, J. S. Héron, S. Sahoo, H. Berger, and A. Kis, "Visibility of dichalcogenide nanolayers," Nanotechnology **22**, 125706 (2011).
10. B. Radisavljevic, A. Radenovic, J. Brivio, V. Giacometti, and A. Kis, "Single-layer MoS_2 transistors," Nat. Nanotechnol. **6**, 147-150 (2011).
11. Y.-H. Lee, X.-Q. Zhang, W. Zhang, M.-T. Chang, C.-T. Lin, K.-D. Chang, Y.-C. Yu, J. T.-W. Wang, C.-S. Chang, L.-J. Li, and T.-W. Lin, "Synthesis of large-area MoS_2 atomic layers with chemical vapor deposition," Adv. Mater. **24**, 2320-2325 (2012).
12. Y. Yu, Y. Yu, Y. Cai, W. Li, A. Gurarslan, H. Peelaers, D. E. Aspnes, C. G. Van de Walle, N. V. Nguyen, Y.-W. Zhang, and L. Cao, "Exciton-dominated dielectric function of atomically thin MoS_2 films," Sci. Rep. **5**, 16996 (2015).
13. S. K. Kang and H. S. Lee, "Study on growth parameters for monolayer MoS_2 synthesized by CVD using solution-based metal precursors," Appl. Sci. Converg. Technol. **28**, 159-163 (2019).
14. R. M. A. Azzam and N. M. Bashara, *Ellipsometry and Polarized Light* (North-Holland Publishing, Amsterdam, 1987).
15. S. Y. Kim, *Ellipsometry* (Ajou University, Suwon, 2000), Chapter 3-4.
16. V. G. Kravets, V. V. Prorok, L. V. Poperenko, and I. A. Shaykevich, "Ellipsometry and optical spectroscopy of low-dimensional family TMDs," Semicond. Phys. Quantum Electron. Optoelectron. **20**, 284-296 (2017).
17. C. Yim, M. O'Brien, N. McEvoy, S. Winters, I. Mirza, J. G. Lunney, and G. S. Duesberg, "Investigation of the optical properties of MoS_2 thin films using spectroscopic ellipsometry," Appl. Phys. Lett. **104**, 103114 (2014).
18. H.-L. Liu, C.-C. Shen, S.-H. Su, C.-L. Hsu, M.-Y. Li, and L.-J. Li, "Optical properties of monolayer transition metal dichalcogenides probed by spectroscopic ellipsometry," Appl. Phys. Lett. **105**, 201905 (2014).
19. T. R. Piwonka-Corle, K. F. Scoffone, X. Chen, L. J. Lacomb, Jr., J.-L. Stehle, D. Zahorski, and J.-P. Rey, "Focused beam spectroscopic ellipsometry method and system," U.S. Patent 5608526A (1997).
20. J. A. Woollam Co., *RC2 Ellipsometer Brochure* (2017). Accessed: April 4, 2020 [Online]. Available: https://www.jawoollam.com/download/pdfs/rc2-brochure.pdf.
21. S. J. Kim and M. H. Lee, "Microspot spectroscopic ellipsometer with 4-reflectors," Korean Patent 10-1922973 (2018).
22. Y. Xiong, Y. Dai, S. Chen, and G. Tie, "Design and experimental demonstration of coaxially folded all-reflective imaging system," Curr. Opt. Photon. **3**, 227-235 (2019).
23. L. Beiser and R. B. Johnson, "Scanners," in *Handbook of Optics*, 2nd ed., M. Bass, ed. (McGraw-Hill, NY, 1995), Chapter 19.
24. S. J. Kim, H. K. Yoon, M. H. Lee, S. J. Ii, S. Y. Cho, Y. H. Kwon, B. K. Kim, D. H. Bae, J. H. Shin, and S. Y. Kim, "Development and evaluation of micro spot spectroscopic ellipsometer," in Proc. *8th International Conference on Spectroscopic Ellipsometry* (Barcelona, Spain, May 2019), p. 152.